# Physics performances for Scalar Electrons, Scalar Muons and Scalar Neutrinos searches at CLIC

Jean-Jacques Blaising[1], Marco Battaglia[2], John Marshall[3], Jacopo Nardulli[4], Mark Thomson[3], Andre Sailer[4] and Erik van der Kraaij[4]

1- Laboratoire d'Annecy-le-Vieux de Physique des Particules, Annecy-le-Vieux - France

2- University of California at Santa Cruz, Santa Cruz, CA - USA

3- University of Cambridge, Cambridge - UK

4- CERN, Geneva - Switzerland

The determination of scalar leptons and gauginos masses is an important part of the program of spectroscopic studies of Supersymmetry at a high energy linear collider. In this talk we present results of a study of the processes: $e^+e^- \to \tilde{e}^+_R\, \tilde{e}^-_R \to e^+e^-\ \tilde{\chi}^0_1\ \tilde{\chi}^0_1$, $e^+e^- \to \tilde{\mu}^+_R\, \tilde{\mu}^-_R \to e^+e^-\ \tilde{\chi}^0_1\ \tilde{\chi}^0_1$, $e^+e^- \to \tilde{e}^+_L\, \tilde{e}^-_L \to e^+\ e^-\ \tilde{\chi}^0_2\ \tilde{\chi}^0_2$ and $e^+e^- \to \tilde{\nu}_e\, \tilde{\nu}_e \to e^+\ e^-\ \tilde{\chi}^+_1\ \tilde{\chi}^-_1$ in a Supersymmetric scenario at 3 TeV at CLIC. We present the performances on the lepton energy resolution and report the expected accuracies on the production cross sections and on the $\tilde{e}_R$, $\tilde{\mu}_R$, $\tilde{\nu}_e$, $\tilde{\chi}^\pm_1$ and $\tilde{\chi}^0_1$ mass determination.

## 1 Introduction

One of the main objectives of linear collider experiments is the precision spectroscopy of new particles predicted in theories of physics beyond the Standard Model (SM), such as Supersymmetry (SUSY). In this talk, we discuss the production of the supersymmetric partners of the muon, electron and neutrino within the so-called constrained Minimal Supersymmetric extension of the SM (cMSSM). The parameters chosen are such that the lightest neutralino has a mass of 340 GeV, the charginos and heavier neutralinos have masses in the range 643 to 917 GeV, the right handed selectron and smuon have a mass of 1010.8 GeV, the left handed selectron and the sneutrino have masses of 1110.4 GeV and 1097.2 GeV respectively. Smuons are produced in pair through $s$-channel $\gamma$/Z exchange, selectrons and sneutrinos are pair produced through $s$-channel $\gamma$/Z exchange or $t$-channel $\tilde{\chi}^0_1$ and $\tilde{\chi}^\pm_1$ exchange respectively. The branching ratio $\tilde{\ell}^\pm_R \to \ell^\pm\ \tilde{\chi}^0_1$ is $\sim 100$ %, and the branching ratios: $\tilde{\mathrm{e}}_\mathrm{L} \to \mathrm{e}^-\ \tilde{\chi}^0_1$, $\tilde{\mathrm{e}}_\mathrm{L} \to \mathrm{e}^-\ \tilde{\chi}^0_2$, and $\tilde{\nu}_\mathrm{e} \to \mathrm{e}^-\ \tilde{\chi}^+_1$ are 16%, 29% and 56% respectively. The cross sections, the decay channels and the cross sections times the branching ratio of the signal processes under study are given in Table 1.

| Process | $\sigma$ fb | Decay Mode | $\sigma \times Br$ fb | $\sigma \times Br(ee4Q)$ fb |
|---|---|---|---|---|
| $e^+e^- \to \tilde{\mu}^+_R\tilde{\mu}^-_R$ | 0.7 | $\mu^+\mu^-\tilde{\chi}^0_1\tilde{\chi}^0_1$ | 0.7 | |
| $e^+e^- \to \tilde{e}^+_R\tilde{e}^-_R$ | 6.1 | $e^+e^-\tilde{\chi}^0_1\tilde{\chi}^0_1$ | 6.1 | |
| $e^+e^- \to \tilde{e}^+_L\tilde{e}^-_L$ | 3.06 | $e^+e^-\tilde{\chi}^0_2\tilde{\chi}^0_2 \to e^+e^-h^0/Z^0h^0/Z^0\tilde{\chi}^0_1\tilde{\chi}^0_1$ | 0.25 | 0.16 |
| $e^+e^- \to \tilde{\nu}_e\tilde{\nu}_e$ | 13.7 | $e^+e^-\tilde{\chi}^\pm_1\tilde{\chi}^\pm_1 \to e^+e^-W^+W^-\tilde{\chi}^0_1\tilde{\chi}^0_1$ | 4.30 | 1.82 |

Table 1: Signal processes, cross sections ($\sigma$), decay modes, cross sections times branching ratio ($\sigma \times Br$) and cross sections times branching ratio into two electrons and four quarks. ($\sigma \times Br(ee4Q)$ ).

For the processes $e^+e^- \to \tilde{\ell}^+_R\tilde{\ell}^-_R$ each $\tilde{\ell}^\pm$ decays into a SM lepton and a $\tilde{\chi}^0_1$; the experimental signature is two oppositely charged leptons plus missing energy. For the processes $e^+\ e^- \to \tilde{e}^+_L\ \tilde{e}^-_L \to e^+\ e^-\ \tilde{\chi}^0_2\ \tilde{\chi}^0_2 \to e^+\ e^-\ \tilde{\chi}^0_1\ \tilde{\chi}^0_1\ h^0\ h^0$ and $e^+e^- \to \tilde{\nu}_e\ \tilde{\nu}_e \to e^+\ e^-\ \tilde{\chi}^+_1\ \tilde{\chi}^-_1 \to e^+\ e^-\ \tilde{\chi}^0_1\ \tilde{\chi}^0_1\ W^+\ W^-$, the signature is a pair $e^+e^-$, four jets and missing energy. The measurement of the lepton energy distributions of these four processes allows to determine their production cross sections and the $\tilde{e}_R,\ \tilde{\mu}_R,\ \tilde{\nu}_e,\ \tilde{\chi}^\pm_1$ and $\tilde{\chi}^0_1$ masses. The aim of this study is study, done for the CLIC CDR [1] is to assess the accuracy, which could be obtained on the mass measurements and on the production cross sections and characterize the detector performances, namely lepton energy resolution.

## 2 Event Simulation and Reconstruction

SUSY signal events and SM background events are generated using WHIZARD 1.94 [2] which was interfaced to PYTHIA 6.4 [3] for fragmentation and hadronization. The simulation is performed using the GEANT4-based [4] MOKKA program [5] with the CLIC_ILD_CDR detector geometry [1], which is based on the ILD detector concept [6] being developed for the ILC. The physics backgrounds simulated for this study are listed in Table 2. The centre-of-

| Process | Decay mode | $\sigma \times Br$ fb | $\sigma \times Br$ fb |
|---|---|---|---|
| | | no cuts | cuts |
| $e^+e^- \to \mu^+\mu^-$ | $\mu^+\mu^-$ | 81.9 | 0.6 |
| $e^+e^- \to \mu^+\nu_e\mu^-\nu_e$ | $\mu^+\mu^-$ | 65.6 | 3.5 |
| $e^+e^- \to \mu^+\nu_\mu\mu^-\nu_\mu$ | $\mu^+\mu^-$ | 6.2 | 2.2 |
| $e^+e^- \to \mathrm{W^+\nu W^-\nu}$ | $\mu^+\mu^-$ | 92.6 | 2.4 |
| $e^+e^- \to \mathrm{Z^0\nu Z^0\nu}$ | $\mu^+\mu^-$ | 40.5 | 0.002 |
| $e^+e^- \to$ All SUSY $-(\tilde{\mu}^+_R\tilde{\mu}^-_R)$ | $\mu^+\mu^-$ | 0.31 | 0.31 |
| $e^+e^- \to e^+e^-$ | $e^+e^-$ | 6226.1 | 77.1 |
| $e^+e^- \to e^+\nu_e e^-\nu_e$ | $e^+e^-$ | 179.3 | 91.1 |
| $e^+e^- \to \mathrm{W^+\nu W^-\nu}$ | $e^+e^-$ | 92.6 | 2.4 |
| $e^+e^- \to \mathrm{Z^0\nu Z^0\nu}$ | $e^+e^-$ | 40.5 | 0.002 |
| $e^+e^- \to$ All SUSY $-(\tilde{\mathrm{e}}^+_\mathrm{R}\tilde{\mathrm{e}}^-_\mathrm{R})$ | $e^+e^-$ | 1.04 | 1.04 |
| $e^+e^- \to \mathrm{W^+W^-Z^0}$ | $e^+e^-W^+W^-$ | 1.35 | 0.61 |
| $e^+e^- \to \mathrm{Z^0Z^0Z^0}$ | $e^+e^-Z^0Z^0$ | 0.045 | 0.023 |
| $e^+e^- \to$ SUSY $-$ ($\tilde{\mathrm{e}}^+_\mathrm{L}\tilde{\mathrm{e}}^-_\mathrm{L}$ and $\tilde{\nu}_\mathrm{e}\tilde{\nu}_\mathrm{e}$) | $\mathrm{e^+e^-}$(WW, $\mathrm{h^0h^0}$, $\mathrm{Z^0Z^0}$) | 0.77 | 0.12 |

Table 2: Background processes, decay modes and cross sections times branching ration, $\sigma \times Br$, without and with preselection cuts.

mass energy spread coming from the momentum spread in the linac and the beamstrahlung is included using the GUINEAPIG [7] beam simulation for the CDR accelerator parameters [8]. It is used as input of WHIZARD in which initial state radiation and final state radiation (FSR) are enabled. An integrated lumnosity of 2000 fb$^{-1}$ was assumed, corresponding to $\simeq$3.5 years (1 year = $10^7$ s) of run at the nominal CLIC luminosity of $5.9\times10^{34}$ cm$^{-2}$s$^{-1}$. Events are subsequently reconstructed using the MARLIN reconstruction program [9]. The track momenta and calorimeter data are input to the PandoraPFA algorithm [10] which performs particle identification and returns the best estimate for the momentum and energy

of the particles. The muon and electron average identification efficiency are 99% and 96% respectively [1]. After reconstruction preselection cuts are applied on the signal samples. Table 3 shows the reconstruction efficiencies, $\epsilon_{\rm R}$, for the signal processes.

| Process | Decay Mode | $\epsilon_R$ No $\gamma\gamma \to h$ | $\epsilon_R$ $\gamma\gamma \to h$ | $\epsilon_S$ |
|---|---|---|---|---|
| $e^+e^- \to \tilde{\mu}^+_R\tilde{\mu}^-_R$ | $\mu^+\mu^-\tilde{\chi}^0_1\tilde{\chi}^0_1$ | 0.975 | 0.965 | 0.97 |
| $e^+e^- \to \tilde{e}^+_R\tilde{e}^-_R$ | $e^+e^-\tilde{\chi}^0_1\tilde{\chi}^0_1$ | 0.946 | 0.902 | 0.94 |
| $e^+e^- \to \tilde{e}^+_L\tilde{e}^-_L$ | $e^+e^-\tilde{\chi}^0_2\tilde{\chi}^0_2 \to e^+e^-h^0/Z^0h^0/Z^0\tilde{\chi}^0_1\tilde{\chi}^0_1$ | 0.67 | 0.63 | 0.94 |
| $e^+e^- \to \tilde{\nu}_e\tilde{\nu}_e$ | $e^+e^-\tilde{\chi}^\pm_1\tilde{\chi}^\pm_1 \to e^+e^-W^+W^-\tilde{\chi}^0_1\tilde{\chi}^0_1$ | 0.49 | 0.46 | 0.94 |

Table 3: reconstruction efficiency, $\epsilon_R$ without and with $\gamma\gamma$ overlay and selection efficiencies $\epsilon_S$ for the different signal processes. The statistical error on these efficiencies is $\sim 1\%$

For the process $e^+e^- \to \tilde{\mu}^+_R\tilde{\mu}^-_R$ there is an inefficiency of about 2.5%; 2.0% is due to the cut on the lepton angle and 0.5% is coming from muon misidentification. For the process $e^+e^- \to \tilde{e}^+_R\tilde{e}^-_R$ there is an inefficiency of 5.4%; 4.1% is due to the cut on the lepton angle and 1.3% is coming from electron misidentification. For the processes $e^+e^- \to \tilde{e}^+_L\tilde{e}^-_L$ and $e^+e^- \to \tilde{\nu}_e\tilde{\nu}_e$, the parton topology signature required is two leptons and four quarks. After reconstruction of all the particles in the event, the jet finder program FASTJET [11] is used to reconstruct jets. The jet algorithm used is the inclusive anti-kt method [12] requiring a minimum jet energy of 20GeV. An event is retained if 6 jets are found and if two of the jets are identified as isolated leptons. Table 3 shows the reconstruction efficiencies of both processes, $\epsilon_{\rm R}$ is the number of reconstructed 6 jet events, with two leptons, divided by the number of generated events with two leptons and four quarks. The energy of the lepton is reconstructed from the momentum of the charged particle track corrected for final state radiation and bremsstrahlung; the energy of photons or $e^+e^-$ pairs from conversions within a cone of 20° around the reconstructed lepton direction is added to the track momentum. The lepton energy resolution is characterized using: $\delta E/E^2_{\rm True}$, where $\delta E = E_{\rm True} - E_{\rm Reco}$, $E_{\rm True}$ is the lepton energy at generator level, before final state radiation or bremsstrahlung and $E_{\rm Reco}$ is the reconstructed lepton energy with photon radiation corrections. Figure 1 shows the lepton energy resolutions, for the four processes, the distributions are fitted using two Gaussian functions. For the muon final state process, the energy resolution of the peak distribution is $\delta E/E^2_{\rm True} = 1.5 \times 10^{-5}$, the energy resolution of the second distribution is $\delta E/E^2_{\rm True} = 4.9 \times 10^{-5}$ and the number of events in the tails is small, 4.1%. For the electron final state processes, the energy resolution of the peak distribution is also $\delta E/E^2_{\rm trueTrue} = 1.5 \times 10^{-5}$, but the energy resolution of the second Gaussian is worse, due to significant photon radiation, $\delta E/E^2_{\rm True} = 8.1 \times 10^{-5}$ and the number of events in the tails is $\sim 30$ %. Despite the presence of four jets, the electron energy resolution for the processes with two electrons and four jets, Figure 1 (c) and (d), is similar to the one of the process with only two electrons in the final state, Figure 1 (b). To investigate the effect of beam induced backgrounds, the reconstruction software is run, overlaying particles produced by $\gamma\gamma \to$ hadrons interactions [1]. A sample of $\gamma\gamma \to$ hadrons events was generated with Pythia and simulated. For each physics event the equivalent of 60 bunch crossings of $\gamma\gamma \to$ hadrons events are selected. The detector hits from these events are merged with those from the physics event before the reconstruction. A time window of 10 nsec on the detector integration time is applied for all detectors, except for the HCAL barrel for which the window is 100

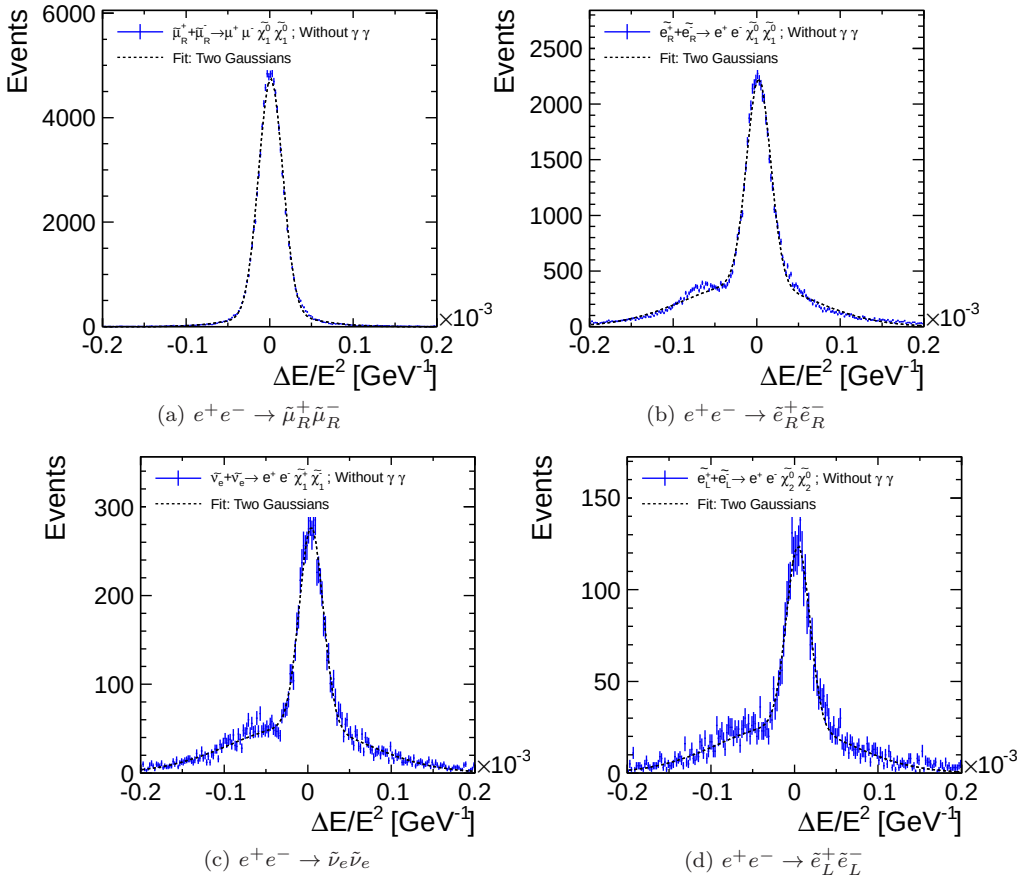


(a) $e^+e^- \to \tilde{\mu}_R^+\tilde{\mu}_R^-$ (b) $e^+e^- \to \tilde{e}_R^+\tilde{e}_R^-$

(c) $e^+e^- \to \tilde{\nu}_e\tilde{\nu}_e$ (d) $e^+e^- \to \tilde{e}_L^+\tilde{e}_L^-$

Figure 1: Lepton energy resolution, for the processes: $e^+e^- \to \tilde{\mu}_R^+\tilde{\mu}_R^-$ (a), $e^+e^- \to \tilde{e}_R^+\tilde{e}_R^-$ (b), $e^+e^- \to \tilde{\nu}_e\tilde{\nu}_e$ (c) and $e^+e^- \to \tilde{e}_L^+\tilde{e}_L^-$ (d)

nsec. After particle reconstruction timing cuts in the range of 1 to 3 nsec are applied in order to reduce the number of particles coming from $\gamma\gamma \to$ hadrons interactions. The cut values vary according to the particle type, (photon, neutral hadron, charged particle), the detector region, (central, forward) and the $P_T$ of the particle. Table 3 shows the reconstruction efficiencies, without overlay and with overlay, after application of the selection cuts. The time selection cuts preserve the energy resolution, but induce an inefficiency of 6% for the dielectron final state processes, 0.5% is coming from the current pattern recognition and tracking software, the rest is due to the increase of lepton misidentification. For the processes $e^+e^- \to \tilde{\mu}_R^+\tilde{\mu}_R^-$ and $e^+e^- \to \tilde{e}_R^+\tilde{e}_R^-$, no timing cuts are applied. The energy resolution of these processes is not affected by the $\gamma\gamma \to$ hadrons interactions because the high $P_T$ cut of 4 GeV, applied to reduce the SM physics background, removes all the hadrons coming from these interactions; it induces a reconstruction inefficiency of 1.0% and 4.6% respectively, see Table 3.

## 3 Event Selection and Mass Determination

To tell apart signal events from background events the following set of discriminating variables is used: dilepton energy $\mathrm{E(L1)+E(L2)}$, vector sum $\mathrm{P_T(L1)+P_T(L2)}$, algebric sum $\mathrm{P_T(L1)+P_T(L2)}$, dilepton invariant mass $\mathrm{M(L1,L2)}$, dilepton velocity $\beta(\mathrm{L1,L2})$, angle of the dilepton missing momentum vector $\cos\theta(\mathrm{L1,L2})$, dilepton acolinearity $\pi-\theta_2-\theta_1$, dilepton acoplanarity $\pi-\phi_2-\phi_1$ and energy imbalance $\Delta=|\mathrm{E(L1)-E(L2)}|/|\mathrm{E(L1)+E(L2)}|$ where L1 and L2 are the two leptons. Histograms of the discriminating variables are built for signal and background events. The events are weighted such that the data samples correspond to the same integrated luminosity. From these histograms, signal and background event probability density functions are computed and combined into a total probability classifier using the multivariate analysis toolkit, TMVA [13]. The signal and background samples are split into two equal event samples called "Monte Carlo" and "Data". The Monte Carlo sample is used to train the classifier which ranks events to be signal or background like. The method is then applied to the so called Data sample, for each event a total probability is computed and a cut is applied to tell apart signal from background. The cut value is chosen to optimise the significance $\mathrm{N_S}/\sqrt{(\mathrm{N_S+N_B})}$ versus the signal efficiency; $\mathrm{N_S}$ and $\mathrm{N_B}$ are the number of signal and background events. The selection efficiencies, $\epsilon_\mathrm{S}$ are shown in Table 3. After selection and background subtraction, the slepton, neutralino or chargino masses are extracted from the position of the kinematic edges of the lepton energy distribution, a technique first proposed for squarks [14], then extensively applied to sleptons [15].

$$m_{\tilde{\ell}^\pm}=\frac{\sqrt{s}}{2}\left(1-\frac{(E_H-E_L)^2}{(E_H+E_L)^2}\right)^{1/2}\ \text{ and }\ m_{\tilde{\chi}_1^0}\text{ or }m_{\tilde{\chi}_1^\pm}=m_{\tilde{\ell}^\pm}\left(1-\frac{2(E_H+E_L)}{\sqrt{s}}\right)^{1/2} \quad (1)$$

The masses depend on the centre-of mass energy $\sqrt{s}/2$ and on the kinematic edges values $E_{L,H}$, therefore the accuracy on the masses relies on the measurement of the shape of the luminosity spectrum and on the lepton energy resolution. The masses are determined using a 2-parameter, $m_{\tilde{\ell}^\pm}$ and $m_{\tilde{\chi}_1^0}$, $\chi^2$ fit to the reconstructed energy distribution. The fit is performed with the MINUIT minimization package [16]. The lepton energy spectrum is a uniform distribution with end points fixed by the slepton and neutralino masses. For each event a random value of $\sqrt{\mathrm{s}}$ is generated taking into account the beamstrahlung and ISR effects; the lepton energy resolution is included using the energy resolution functions shown in Figure 1. The process cross section is obtained from the integral of the momentum distribution. Table 4 shows the values of the measured sleptons cross sections, sleptons masses and gauginos masses. Figure 2 (a) and (b) show the lepton energy distributions and fit results for the processes, $e^+e^-\to\tilde{\mu}_R^+\tilde{\mu}_R^-$ and $e^+e^-\to\tilde{\nu}_e\tilde{\nu}_e$ respectively. For the process $e^+e^-\to\tilde{e}_L^+\,\tilde{e}_L^-\to e^+\,e^-\,\tilde{\chi}_2^0\,\tilde{\chi}_2^0$, the cross section is determined from the fit to Di-jet invariant mass shown in Figure 2 (c).

## 4 Acknowledgments

We are grateful to Daniel Schulte for making the luminosity spectrum and generated $\gamma\gamma\to$ hadrons events available as well as for the useful discussions about the luminosity control.

| Process | Decay Mode | $\sigma$ fb | $m_{\tilde{\ell}}$ GeV | $m_{\tilde{\chi}_1^0}$ or $m_{\tilde{\chi}_1^\pm}$ GeV |
|---|---|---|---|---|
| $e^+e^- \to \tilde{\mu}_R^+\tilde{\mu}_R^-$ | $\mu^+\mu^-\tilde{\chi}_1^0\tilde{\chi}_1^0$ | 0.71 ± 0.02 | 1014.3 ± 5.6 | 341.8 ± 6.4 |
| $e^+e^- \to \tilde{e}_R^+\tilde{e}_R^-$ | $e^+e^-\tilde{\chi}_1^0\tilde{\chi}_1^0$ | 6.20 ±0.05 | 1001.6 ± 2.8 | 340.6 ± 3.4 |
| $e^+e^- \to \tilde{e}_L^+\tilde{e}_L^-$ | $e^+e^-\tilde{\chi}_2^0\tilde{\chi}_2^0$ | 2.77 ± 0.20 | | |
| $e^+e^- \to \tilde{\nu}_e\tilde{\nu}_e$ | $e^+e^-\tilde{\chi}_1^\pm\tilde{\chi}_1^\pm$ | 13.24 ± 0.32 | 1096.4 ±3.9 | 644.8 ± 3.7 |

Table 4: Cross sections values, sleptons and gauginos masses and statistical accuracies.

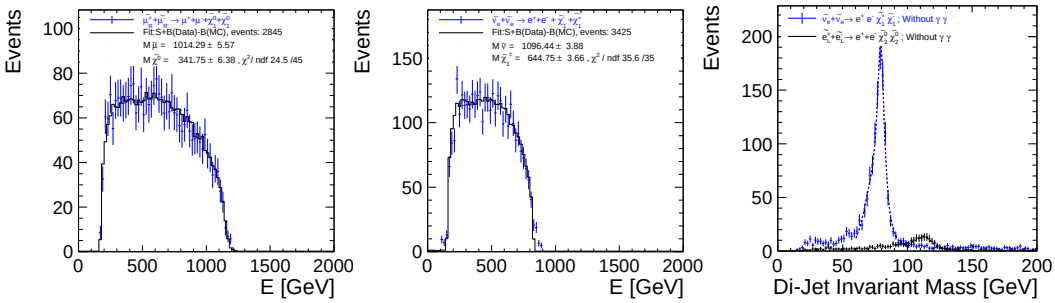


(a) $e^+e^- \to \tilde{\mu}_R^+\tilde{\mu}_R^-$ (b) $e^+e^- \to \tilde{\nu}_e\tilde{\nu}_e$ (c) $e^+e^- \to \tilde{\nu}_e\tilde{\nu}_e$ and $e^+e^- \to \tilde{e}_L^+\tilde{e}_L^-$

Figure 2: Lepton energy spectrum and fit results, for the processes: (a) $e^+e^- \to \tilde{\mu}_R^+\tilde{\mu}_R^-$, (b) $e^+e^- \to \tilde{\nu}_e\tilde{\nu}_e$, (c) Di-jet invariant for $e^+e^- \to \tilde{\nu}_e\tilde{\nu}_e$ and $e^+e^- \to \tilde{e}_L^+\tilde{e}_L^-$

## References


[1] Physics and Detectors at CLIC, Conceptual Design Report, https://edms.cern.ch/document/1160419

[2] W. Kilian, T. Ohl, J. Reuter, WHIZARD: Simulating Multi-Particle Processes at LHC and ILC , arXiv: 0708.4233 [hep-ph].

[3] T. Sjostrand, S. Mrenna and P. Z. Skands, JHEP **0605** (2006) 026 [arXiv:hep-ph/0603175].

[4] S. Agostinelli *et al.* [GEANT4 Collaboration], Nucl. Instrum. Meth. A **506** (2003) 250.

[5] P. Mora de Freitas, in Proc. of the *Int. Conf. on Linear Colliders (LCWS 04)* vol. 1 (2004) 441.

[6] The International Large Detector: Letter of Intent, 2010, http://arxiv.org/pdf/1006.3396v1, ILD Concept Group - Linear Collider

[7] D. Schulte, TESLA Note 97-08.

[8] H. Braun *et al.* [CLIC Study Team], CLIC-NOTE-764 (2008).

[9] F. Gaede, Nucl. Instrum. Meth. A **559** (2006) 177.

[10] Thomson, M. A., Nucl. Particle Flow Calorimetry and the PandoraPFA Algorithm, Instrum.Meth. A611:25-40,2009

[11] M. Cacciari, G. P. Salam and G. Soyez, "The anti-kt jet clustering algorithm", JHEP 0804 (2008) 063 [arXiv:0802.1189].

[12] M. Battaglia, P. Ferrari, A Study of $e^+e^- \to H^0A^0 \to b\bar{b}b\bar{b}$ at 3 TeV at CLIC, LCD-2010-006

[13] A. Hoecker, P. Speckmayer, J. Stelzer, J. Therhaag, E. von Toerne, and H. Voss, "TMVA: Toolkit for Multivariate Data Analysis," PoS A CAT 040 (2007) [physics/0703039].

[14] J. L. Feng and D. E. Finnell, Phys. Rev. D **49** (1994) 2369 [arXiv:hep-ph/9310211].

[15] H. U. Martyn and G. A. Blair, arXiv:hep-ph/9910416.

[16] F. James and M. Roos, Comput. Phys. Commun. **10** (1975) 343.